CHEMICAL ENGINEERING TRANSACTIONS
VOL. 100, 2023
A publication of AIDIC
The Italian Association of Chemical Engineering
Online at www.cetjournal.it
Guest Editors: Sauro Pierucci, Flavio Manenti

ISBN 979-12-81206-03-8; **ISSN** 2283-9216
DOI: 10.3303/CET23100057

Experimental and Computational Study of Supercritical Fluid Extraction (SFE) of Omega-3 Components from Fish Oil in Structured Packing

Luca Schembri, Giuseppe Caputo, Michele Ciofalo, Franco Grisafi, Serena Lima, Francesca Scargiali*

Università degli Studi di Palermo, Dipartimento di Ingegneria, Edificio 6, Viale delle Scienze 90128
francesca.scargiali@unipa.it

The benefits of polyunsaturated fatty acids and their implications for human health have gained scientific attention to their extraction from biological sources, not being produced by the human body. Most known industrial productions of omega-3 fatty acids often work under operating conditions that may degrade these components and they often use toxic or flammable solvents that can adversely affect human health. In this sense, innovative and interesting prospects are provided by Supercritical Fluid Extraction (SFE).
In this work, two parallel studies were carried out: an experimental activity in a laboratory apparatus using supercritical carbon dioxide ($scCO_2$) and preliminary computational fluid dynamics (CFD) simulations, limited to the hydrodynamic aspects of the process. In the experimental apparatus a *Sulzer*® EX structured packing, made up of corrugated metal gauze sheets, was used as the column filler. The study made it possible to identify the optimal operating conditions leading to an enrichment of the starting mixture in Eicosapentaenoic acid (EPA) and Docosahexaenoic acid (DHA), target products. CFD simulations were based on the *Volume of Fluid (VOF)* approach, suitable to the present complex multiphase system with two phases in close contact (transesterified fish oil and $scCO_2$). The meatus created by the corrugations of the metal gauze was chosen as the calculation domain representative of the system. The computations were performed by the commercial software *Ansys Fluent*®, which allowed the prediction of the hydrodynamic evolution of the system through transient simulations. CFD predictions were in qualitative agreement with the experimental results.

1. Introduction

The growing attention to the health and psycho-physical well-being of humans and the optimistic evaluation of the benefits associated with the intake of omega-3 caused a global increase in the demand for products containing Poly-Unsaturated Fatty Acids (PUFA). For its market, estimated in 2021 equals to 2.19 billion dollars, a forecast of increase, for the period 2022-2030, is expected with a Compound Annual Growth Rate (CAGR) of 8.0% (Polaris, 2022). In previous years awareness policies were implemented by the various governments like USA and Europe to influence the trend of the demand of these compounds. The interest in PUFAs arises from the variety of biochemical processes in which they are involved. Numerous studies have reported physiological effects of PUFA, in fact omega-3 may influence several pathological conditions associated with metabolic, inflammatory and oxidative processes. PUFAs may regulate the antioxidant signaling pathway and modulate inflammatory processes. They also influence hepatic lipid metabolism and physiological responses of other organs, including the heart (Djuricic & Calder, 2021). The Omega-3 product industry is driven by the growing demand in the Active Pharmaceutical Ingredient (API) market, linked to the growing awareness of the effective action of these products, in particular on chronic and cardiovascular diseases.
Nowadays one of the problems of extraction and purification is linked to the fact that known industrial processes work under operating conditions that inevitably induce the degradation of these components and the use of toxic or flammable solvents that can have adverse effects on human health, as well as for the environment. In this sense, liquid-solvent extraction, that makes use of CO_2 in supercritical conditions as a solvent, offers innovative, attractive and more environmentally friendly chances.

Paper Received: 26 January 2023; Revised: 19 March 2023; Accepted: 30 May 2023
Please cite this article as: Schembri L., Caputo G., Ciofalo M., Grisafi F., Lima S., Scargiali F., 2023, Experimental and Computational Study of Supercritical Fluid Extraction (SFE) of Omega-3 Components from Fish Oil in Structured Packing, Chemical Engineering Transactions, 100, 337-342 DOI:10.3303/CET23100057

Supercritical conditions are used throughout the process to increase the CO_2's solvating power. The Omega-3 industry is commonly divided into two categories, based on the origin of the raw material (marine sources and plant sources) (Lima et al., 2020, 2022).
One of the possible starting matrices is an oil obtained from waste of the fishing industry such as tuna, sardines, or shark. The problem with this matrix is that more than 40 different fatty acids are present in these oils, which makes them a much more complex and articulated mixture (Wen et al., 2023). In fact, that mixtures consist of linear chain fatty acids having 14 to 22 carbon atoms, with several unsaturations typically ranging from 0 up to 6. Another problem is the lack in the literature of studies and models of the Supercritical Fluid Extraction (SFE) phenomenon that would allow a more optimal separation without the need to work with an energy-intensive plant at high pressures. This work takes part on the aforementioned aspects by proposing a fluid dynamics computational study to optimize the enrichment of the matrix in compounds with high added value.

2. Experimental methods and materials

There are several methods traditionally used for Omega-3 concentration and purification such as urea adduction, chromatographic methods, fractional crystallization at low temperatures, distillation, enzymatic and integrated methods and SFE (Caputo et al., 2016). The last one, employing a continuous operating equipment, is based on the pioneering experiments carried out by Brunner and co-workers (Riha & Brunner, 2000). In the last twenty years, there have been many improvements in this process, which has increasingly taken hold in the world of industry since it guarantees a product with high purity and thermally undegraded (Abou Elmaaty et al., 2022). Figure 1 shows the process flow diagram of the pilot plant where the present experimental activities were conducted. The plant is equipped with a 2.40 m active height extraction column (T-1). The column has an inner diameter of 21.2 mm and is filled with a Sulzer® EX packing layer. Liquid CO_2 at 40 bar, stored in vessel S-2, is compressed via pump P-2 to the supercritical state at 145 bar (extraction pressure). The $scCO_2$ is heated using a hairpin heat exchanger (H-3) to the desired temperature of 60 °C. Afterwards, the CO_2 enters the extraction column from the bottom and leaves it from the top, where it is expanded to 40 bar by a manual backpressure regulator valve entering the separation vessel S-1. Here the extracted compound can be removed by a needle valve from the bottom of the vessel. The gaseous CO_2 flows through a plate condenser (C-1) back into the CO_2 vessel (S-2). The single-phase flow rate of the $scCO_2$ was measured by a flowmeter Bronkhorst®, mini CORI-FLOW® Series, model M14 with a nominal range between 0.1 e 30 kg h^{-1} and a mass flow accuracy for liquids of ±0,2%. The oil phase is fed into the central region of the column via pump P-1 and, after being processed, is taken from the system as a fraction enriched in the heavier components in the bottom of the column and as a light fraction from the bottom of the S-1 tank. A part of this is fed back into the column as a reflux current using pump P-3.

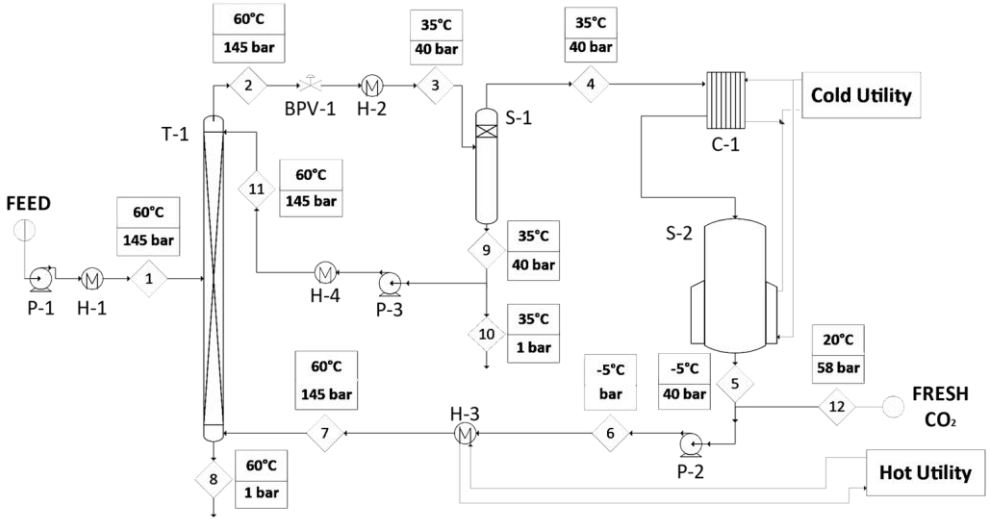

Figure 1 Schematic diagram of the experimental setup and operating conditions for every streamline.

2.1 Determination of physical properties

Simple equations of state are not able to accurately estimate the fluids' properties over the large interval of pressure and temperature of the present study and multi-parameter equations of state are required. In regard to CO_2 density, among several models present in the literature (Bisotti et al., 2019), the most suitable for our case was found to be the Bender equation of state (Brunner, 2013):

$$P = RT\rho_f + B\rho_f^2 + C\rho_f^3 + D\rho_f^4 + E\rho_f^5 + F\rho_f^6 + \left(G + H\rho_f^2\right)\rho_f^3\, exp(-a_{20}\rho_f^2) \quad (1)$$

This equation calculates the pressure of a generic fluid as a function of density using the seven constants B, C, D, E, F, G, H, which in their turn are functions of temperature via 20 parameters, to be fitted on property data and must be inverted to provide the density as a function of pressure and temperature. The Bender equation of state is considered a good compromise between simple and more elaborate equations and it is highly reliable for homogeneous fluids in the supercritical state, particularly for well-known compounds as CO_2 with a low acentric factor (Ghazouani et al., 2005).
For the evaluation of the $scCO_2$ viscosity, the following formula was used (Heidaryan et al., 2011):

$$\mu_v = \frac{\left(A_1 + A_2\rho_f + A_3\rho_f^2 + A_4(\ln(T))^2 + A_6(\ln(T))^3\right)}{1 + A_7\rho_f + A_8\ln(T) + A_9(\ln(T))^2} \quad (2)$$

To evaluate the interfacial tension of marine fatty acid ethyl esters (FAEE), which constitute the fish oil used, in contact with $scCO_2$, the model proposed by Seifried (Seifried & Temelli, 2010) was employed, adapted with a proper corrective factor for the present numeric simulation.

$$\gamma\left(P, T, \rho_{CO_2}\right) = \gamma_0(T) - k_1(T)(P - 0.1) - k_2(T)\left(1 - \exp\left(k_3(T)\left(\rho_{CO_2} - \rho^0_{CO_2}\right)\right)\right) \quad (3)$$

As the contact angle, the value estimated by Fernandes (Fernandes et al., 2009). The thermodynamic properties of transesterified fish oil (*LISY- Ethyl Esters 33/22 HE002*) were experimentally measured under the present operating conditions. For the evaluation of density, a previously calibrated graduated cylinder was filled with the substance and weighted by an analytical balance Kern® ABS-ABJ. The viscosity of fish oil was measured employing an Ubbelohde suspended-level capillary viscometer 532 11 Ia-Schott Mainz-Jena^{ER}Glas (diameter of 0.95 mm) provided with a ViscoClock® instrumentation and immersed in a thermo-static bath Lauda®015T. All data are given in Table 1.

Table 1: Physical properties of $scCO_2$/fish oil for the selected operating conditions (P = 145 bar and T = 60°C).

	$scCO_2$	**Transesterified Fish Oil**
Density [kg m^{-3}]	582.61	884
Viscosity [Pa s]	$4.36\cdot10^{-5}$	$2.72\cdot10^{-3}$
Surface Tension [N m^{-1}]		$5.68\cdot10^{-4}$
Contact Angle [deg]		30

3. Numerical simulation

The VOF formulation models two or more immiscible phases by solving the momentum equations of each of the fluids by using the commercial CFD code *Ansys Fluent*® v.18.1 (ANSYS Inc., 2013). In this study, the VOF model solved the transport equations for two Eulerian phases, $scCO_2$ and transesterified fish oil. The volume fraction is solved by the explicit method, which exhibits a better numerical accuracy compared to the implicit formulation. The maximum Courant number allowed near the free surface is set to 0.25. To model the interface between the two phases, the sharp interface model is used, since a distinct interface is present between the supercritical and the liquid phases. The volume fraction cutoff is set to 10^{-6}. In vector formulation, the momentum (Navier-Stokes) equations solved are:

$$\frac{\partial}{\partial t}(\rho\,\vec{\boldsymbol{u}}) + \nabla\cdot(\rho\,\vec{\boldsymbol{u}}\,\vec{\boldsymbol{u}}) = -\nabla\cdot P + \nabla\cdot[\mu\,(\nabla\,\vec{\boldsymbol{u}} + \nabla\,\vec{\boldsymbol{u}}^T)] + \rho\,\vec{\boldsymbol{g}} + \vec{\boldsymbol{F}} \quad (4)$$

In Eq(4), ρ and $\vec{\boldsymbol{u}}$ define the local density and the velocity vector, μ is the viscosity of the fluid, $\vec{\boldsymbol{g}}$ is the gravitational acceleration vector. P defines the pressure and $\vec{\boldsymbol{F}}$ is the source term. $\vec{\boldsymbol{F}}$ also contains model-dependent source terms. The local density is calculated by:

$$\rho = \alpha_1\,\rho_1 + \alpha_2\,\rho_2 \quad (5)$$

where ρ_q specifies the density of phase q and α_q represents the local volume fraction of phase q. The volume fraction must be solved only for one of the phases, since for the other phase it is determined from the constraint:

$$\sum_{i=1}^{2}\alpha_i = 1 \quad (6)$$

The tracking of the interface between the phases is performed by solving the continuity equation for the volume fraction of one of the phases:

$$\frac{\partial}{\partial t}\left(\alpha_q\,\rho_q\right) + \nabla\cdot\left(\alpha_q\,\rho_q\,\overrightarrow{\boldsymbol{u_q}}\right) = S_{\alpha_q} + \sum_{p=1}^{n}\left(\dot{m}_{pq} - \dot{m}_{qp}\right) \quad (7)$$

$S_{\alpha_q}$is a mass source or mass sink; $\dot{m}_{pq}$ and $\dot{m}_{qp}$ are the mass transfer rates from phase q to phase p and *vice versa*. The continuum surface force (CSF) model proposed by Brackbill (Brackbill et al., 1992) is implemented such that the addition of surface tension to the VOF calculation results in a source term $\vec{\boldsymbol{F}}$ in the momentum equation. For each simulation carried out, the fluids are assumed to be Newtonian, isothermal and

incompressible; hence the properties are kept constant. The values for the thermophysical properties implemented in computational simulations, including the values for the surface tension and contact angle are reported in Table 1.

3.1 Packing geometry and computational domain

Sulzer® EX structured gauze packing and its geometric characteristics are shown in Figure 2.

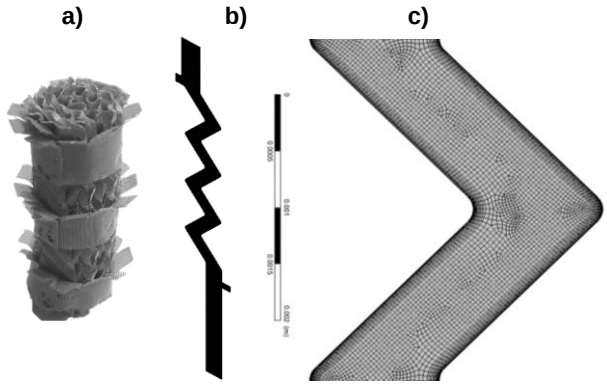

d)

Packing - Sulzer® EX	
Column internal diameter [mm]	21.2
Material	SS. gauze
Fractional void volume, ε	0.86
Specific surface area, a_s [$m^2\ m^{-3}$]	1710
Inclination angle, θ [degrees]	45
Number of gauzes	11

Figure 2: a) Photography of the Sulzer® EX structured gauze packing; b) Computational domain for the fluid dynamics calculations; c) Zoomed detail of the computational mesh; d) Geometric data of the packing.

The characteristic length of the packing is defined by the diameter of its channels, $d_p = 6(1-\varepsilon)/a_s$, where ε is the void fraction and a_s is the surface area per unit volume of packing. The hydraulic diameter, d_h , is defined as $d_h = 4\varepsilon/a_s$.

The calculations were carried out in the computational domain shown in Figure 2.b Its geometry corresponds to the space between two neighboring packing sheets of a packing element. It develops mainly in two dimensions; three volumes were placed along the third direction, so that to make the system three-dimensional in order to be able to use the same model in more complex applications. For simplicity reasons, along the longitudinal direction the computational domain includes only three and a half repetitive crisscross units for a total length of ~10 mm (not including upper and lower headers), while the real equipment includes more than 800 such units and is ~2.4 m high. The grid was refined toward the walls so that at least 12–15 grid points were placed in the liquid film. Structured hexahedral meshes with 60,000, 120,000, 160,000 and 480,000 total volumes (one third of which in the main simulation plane) were tested. Preliminary results showed that the mesh with 160,000 volumes gave the best compromise between the mesh quality (in terms of aspect ratio, orthogonality and uniformity), and the computational burden required by the simulation. The criterion used to choose the mesh was based on the observation of the shape of the liquid film on the solid wall of the packing. While the first two coarser meshes didn't result in the formation of a uniform film on the solid surface, the last two gave results almost identical to each other and in agreement with the expected continuous film behavior, so the 160,000 volumes mesh was chosen. The walls were defined as no-slip boundary conditions. Both the liquid and $scCO_2$ inlet zones were defined as uniform inlet velocity (Dirichlet) boundary conditions. The outlets for $scCO_2$ and liquid were defined as pressure-outlet boundaries with a gauge pressure of 0 Pa.

3.2 Computation details

For the time-dependent CFD a time step of $1 \cdot 10^{-4}$ s was chosen with 30 iterations per time step. The initialization was made with the entire domain filled with $scCO_2$ and as a viscous model, taking into account the low Reynolds number present in the system for both phases, a laminar model was chosen. A phase-coupled PISO algorithm was used to solve the pressure-velocity coupling. The volume fraction was discretized with a compressive scheme, while pressure was discretized with a PRESTO! scheme. The momentum equations were discretized with second-order upwind schemes and the Least Squares Cell Based gradient method was chosen. The simulations were usually protracted up to a real time of about 120 s.

4. Results and discussion

4.1 Experimental results

The experimental activity was carried out in order to investigate the optimal conditions of supercritical extraction. Attention was paid to the flow rate of $scCO_2$ to be sent in the column that allows the best extraction in reference

to the two compounds of interest with high added value: Eicosapentaenoic acid (EPA) and Docosahexaenoic acid (DHA). The best results were obtained with an extraction pressure of 145 bar and a temperature of 60 °C. The transesterified fish oil flow rate was set to 0.90 kg h^{-1} and different solvent flow rate values were investigated. Using a flow rate of 30.00 kg h^{-1} as reported in the literature (Riha & Brunner, 2000), the experiments showed a total lack of product in the refined section and the consequent malfunction of the entire process: the feed was not properly separated into light and heavy compounds as required, but was dragged as a whole into the separation unit downstream of the extraction column. Therefore, the solvent flow rate was gradually reduced; the maximum separation, as verified by chromatographic analysis, was obtained for a value of 9.00 kg h^{-1}. In the corresponding experimental trial, the product was present in the bottom-column and correctly enriched as designed. Different non-intrusive and intrusive techniques have been proposed for measuring the flow patterns inside process equipment (Busciglio et al., 2010), but none of them was applicable to the complexity of our system. To investigate what happened inside the extraction column with the initial flow rate and what changed with the reduced flow rate, a computational fluid dynamics study of the multiphase system was carried out as will be discussed below.

4.2 CFD simulations

The transient simulation illustrated in Figures 3 and 4 was carried out for P=145 bar, T= 60 °C imposing an oil mass flow rate of 0.9 kg h-1 (inlet velocity $1.428 \cdot 10^{-4}$ m s^{-1}). The $scCO_2$ mass flow rate was kept equal to 9.00 kg h^{-1} (inlet velocity $3.098 \cdot 10^{-2}$ m s^{-1}) from t=0 to t=70 s and then was made to increase stepwise to 30 kg h^{-1} (inlet velocity 0.1033 m s^{-1}). The lower (sampling) outlet was opened at t=26 s and closed at t=76 s to mimic the experimental history.

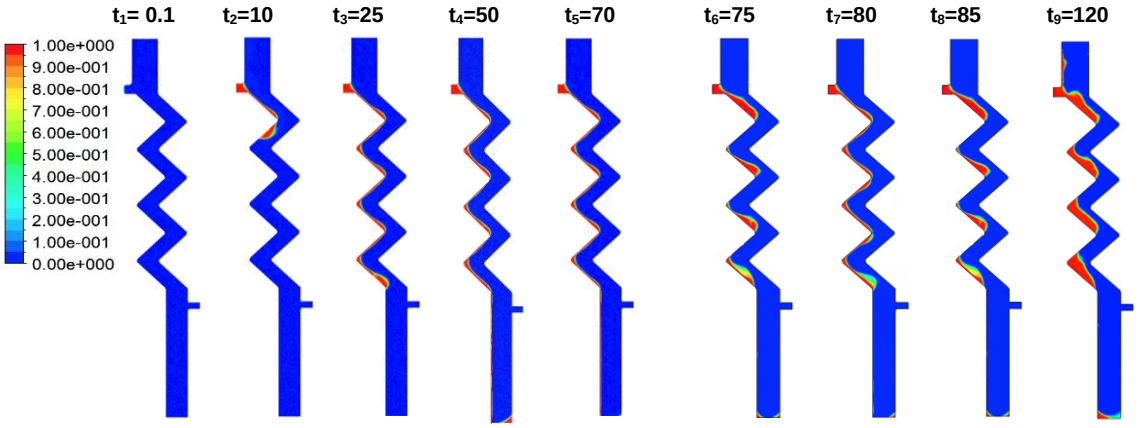

Figure 3: Contours of liquid holdup obtained for P=145 bar, T= 60 °C. Time is expressed in seconds.

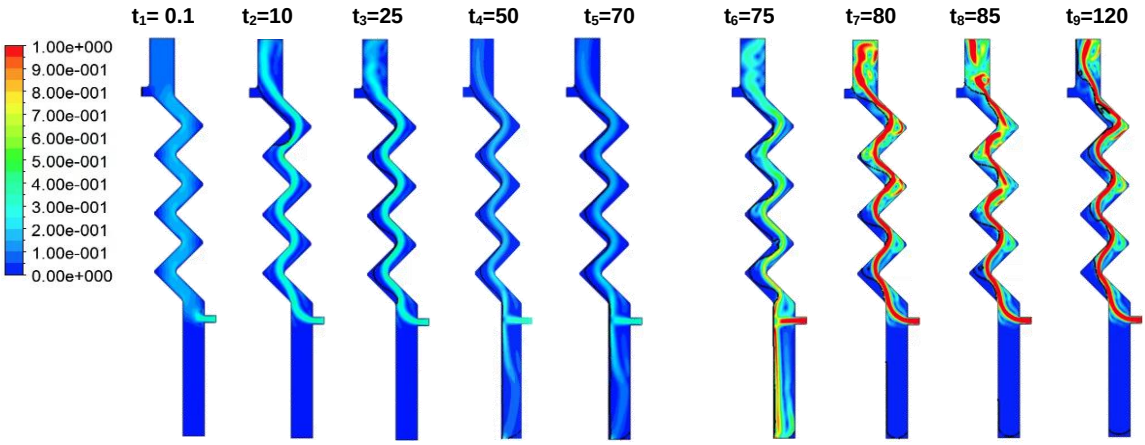

Figure 4: Contours of velocity normalized by the maximum inlet velocity of $scCO_2$ (0.103 m s^{-1}). A thin black line represents the interface. Time is expressed in seconds.

Figure 3 shows the contours of liquid holdup obtained during the whole transient. As it can be seen, in the first part of the transient (instants t_1-t_5), the formation of the film starts at the beginning of the run and the film

progressively and regularly wets the full extent of the packing sheet. In the second part of the transient (instants t_6-t_9) the increase of $scCO_2$ flow rate immediately leads to a thickening of the oil film, previously uniformly distributed, in some areas of the corrugation. Following the closure of the lower (sampling) outlet at t=76 s, the continuity of the film and its normal outflow towards the section bottom are interrupted and the oily phase is entrained towards the upper outlet. This is clearly shown in Figure 4, which reports velocity contours normalized by the inlet-velocity of $scCO_2$ at the highest flow rate.

5. Conclusions

Experimental results for SFE in a column filled with a Sulzer® EX packing were obtained at different $scCO_2$ (solvent) mass flow rates. The best results to maximize the omega-3 extraction were acquired at an extraction pressure of 145 bar, a temperature of 60 °C and a $scCO_2$/oil flow rate ratio of 100. CFD simulations of a simplified version of the experimental system were also carried out to investigate possible fluid-dynamics improvements of the system. Simulation results were in qualitative agreement with the observed behaviour of the system and could predict the transition to flooding conditions. The model can be used in the future to evaluate the optimal operating conditions under a different matrix, a more complex calculation domain and, in conjunction with a predictive model of mass transport, can be used to predict the SFE yield in terms of components with high added value.

References

Abou Elmaaty, T., Sayed-Ahmed, K., Elsisi, H., & Magdi, M. (2022). Optimization of Extraction of Natural Antimicrobial Pigments Using Supercritical Fluids: A Review. *Processes*, *10*(10), 2111.

ANSYS Inc. (2013). ANSYS Fluent Theory Guide. *ANSYS Inc., USA*, *15317*(November), 814. http://www.afs.enea.it/project/neptunius/docs/fluent/html/th/main_pre.htm

Bisotti, F., di Pretoro, A., Dell'Angelo, A., Previtali, D., Amaral, A. F., Andoglu, E. M., & Manenti, F. (2019). Smart implementation of bender equation of state. *Chemical Engineering Transactions*, *74*(June 2018).

Brackbill, J. U., Kothe, D. B., & Zemach, C. (1992). A continuum method for modeling surface tension. *Journal of Computational Physics*, *100*(2), 335–354.

Brunner, G. (2013). Gas Extraction. In *Journal of Chemical Information and Modeling* (Vol. 53, Issue 9).

Busciglio, A., Grisafi, F., Scargiali F., Brucato A. (2010). On the measurement of local gas hold-up and interfacial area in gas–liquid contactors via light sheet and image analysis. *Chemical Engineering Science*, 65(12), 3699–3708.

Caputo, G., Rubio, P., Scargiali, F., Marotta, G., & Brucato, A. (2016). Experimental and fluid dynamic study of continuous supercritical water gasification of glucose. *Journal of Supercritical Fluids*, *107*, 450–461.

Djuricic, I., & Calder, P. C. (2021). Beneficial outcomes of omega-6 and omega-3 polyunsaturated fatty acids on human health: An update for 2021. *Nutrients*, *13*(7).

Fernandes, J., Lisboa, P. F., Simões, P. C., Mota, J. P. B., & Saatdjian, E. (2009). Application of CFD in the study of supercritical fluid extraction with structured packing: Wet pressure drop calculations. *Journal of Supercritical Fluids*, *50*(1), 61–68.

Ghazouani, J., Chouaieb, O., & Bellagi, A. (2005). Evaluation of the parameters of the Bender equation of state for low acentric factor fluids and carbon dioxide. *Thermochimica Acta*, *432*(1), 10–19.

Heidaryan, E., Hatami, T., Rahimi, M., & Moghadasi, J. (2011). Viscosity of pure carbon dioxide at supercritical region : Measurement and correlation approach. *The Journal of Supercritical Fluids*, *56*(2), 144–151.

Lima, S., Lokesh, J., Schulze, P. S. C., Wijffels, R. H., Kiron, V., Scargiali, F., Petters, S., Bernstein, H. C., & Morales-Sánchez, D. (2022). Flashing lights affect the photophysiology and expression of carotenoid and lipid synthesis genes in Nannochloropsis gaditana. *Journal of Biotechnology*, *360*(August), 171–181.

Lima, S., Villanova, V., Grisafi, F., Brucato, A., & Scargiali, F. (2020). Combined effect of nutrient and flashing light frequency for a biochemical composition shift in Nannochloropsis gaditana grown in a quasi-isoactinic reactor. *Canadian Journal of Chemical Engineering*, *98*(9), 1944–1954.

Polaris. (2022). *Omega 3 Market Share, Size, Trends, Industry Analysis Report*. https://www.polarismarketresearch.com/industry-analysis/omega-3-market

Riha, V., & Brunner, G. (2000). Separation of fish oil ethyl esters with supercritical carbon dioxide. *The Journal of Supercritical Fluids*, *17*(1), 55–64.

Seifried, B., & Temelli, F. (2010). Interfacial tension of marine lipids in contact with high pressure carbon dioxide. *Journal of Supercritical Fluids*, *52*(2), 203–214.

Wen, Y.-Q., Xue, C.-H., Zhang, H.-W., Xu, L.-L., Wang, X.-H., Bi, S.-J., Xue, Q.-Q., Xue, Y., Li, Z.-J., Velasco, J., & Jiang, X.-M. (2023). Concomitant oxidation of fatty acids other than DHA and EPA plays a role in the characteristic off-odor of fish oil. *Food Chemistry*, *404* (October 2022), 134724.